

New high temperature furnace for structure refinement by powder diffraction in controlled atmospheres using synchrotron radiation

L. Margulies, M. J. Kramer, and R. W. McCallum

Ames Laboratory, U.S. Department of Energy, and Department of Materials Science and Engineering, Iowa State University, Ames, Iowa 50011-3020

S. Kycia

Cornell High Energy Synchrotron Source (CHESS), Cornell University, Ithaca, New York 14853

D. R. Haeffner and J. C. Lang

Advanced Photon Source (APS), Argonne National Laboratory, Argonne, Illinois 60439

A. I. Goldman

Ames Laboratory, U.S. Department of Energy, and Department of Physics and Astronomy, Iowa State University, Ames, Iowa 50011-3020

(Received 1 March 1999; accepted for publication 13 May 1999)

A low thermal gradient furnace design is described which utilizes Debye–Scherrer geometry for performing high temperature x-ray powder diffraction with synchrotron radiation at medium and high energies (35–100 keV). The furnace has a maximum operating temperature of 1800 K with a variety of atmospheres including oxidizing, inert, and reducing. The capability for sample rotation, to ensure powder averaging, has been built into the design without compromising thermal stability or atmosphere control. The ability to perform high-resolution Rietveld refinement on data obtained at high temperatures has been demonstrated, and data collected on standard Al_2O_3 powder is presented. Time-resolved data on the orthorhombic to rhombohedral solid state phase transformation of SrCO_3 is demonstrated using image plates. Rietveld refinable spectra, collected in as little as 8 s, opens the possibility of performing time-resolved structural refinements of phase transformations. © 1999 American Institute of Physics. [S0034-6748(99)00309-3]

I. INTRODUCTION

Synchrotron radiation has been shown to be an excellent source for high-resolution powder diffraction studies. A number of such studies have shown that reliable structural parameters can be extracted from synchrotron data utilizing Rietveld refinement programs.^{1–5} Most high temperature powder diffraction studies have focused primarily on qualitative phase analysis. Over the years, a number of high temperature diffractometer designs have been reported in the literature.^{6–9} None of these designs, however, allow for sample rotation while maintaining a controlled atmosphere and low thermal gradient across the sample, a requirement that is critical for studying how processing parameters affect high temperature phase transformations and structures. The ability to accurately reproduce a variety of processing conditions is necessary in order to assure a reliable correlation between the high temperature diffraction data and the phase equilibria region of interest. Indeed, most high temperature diffraction designs produce a highly artificial sample environment which is often not representative of the actual processing conditions of interest. This is primarily due to the commonly used strip heater design which has been carried over from its use with conventional tube or rotating anode sources. The nonuniform heating geometry of this design produces significant thermal gradients both laterally and longitudinally across the sample. Additionally, the strip heater

design does not allow for an easy method of introducing sample rotation, which is critical for achieving powder averaging and quantitative structure factor data.

Thermal expansion of the sample and substrate is also a source of error. In the flat plate, Bragg–Brentano geometry a number of geometrical aberrations are introduced as the sample surface deviates from the focusing plane. Thermal expansion during heating will continually shift the sample surface height. This must often be adjusted during the course of sequential data sets, complicating later analysis. For this reason, Debye–Scherrer geometry is preferred for high temperature powder diffraction. With conventional x-ray sources this was often not practical, due primarily to absorption considerations. The use of high energy x-rays from synchrotron sources alleviates this problem and allows for a considerably more robust furnace design. In addition, Debye–Scherrer geometry allows for a more natural introduction of sample rotation into the furnace design.

In constructing a furnace for high-resolution diffraction, there are three primary design goals; (i) due to the logistics of synchrotron work, it is necessary for the furnace to be compact and portable. It must be easily and quickly mounted and aligned on a standard four circle goniometer. (ii) The sample environment must be well controlled and flexible. Thermal gradients must be minimized, and a wide range of temperatures and atmospheres should be achievable. The furnace should also be designed to mimic actual processing conditions that are routinely used in materials preparation.

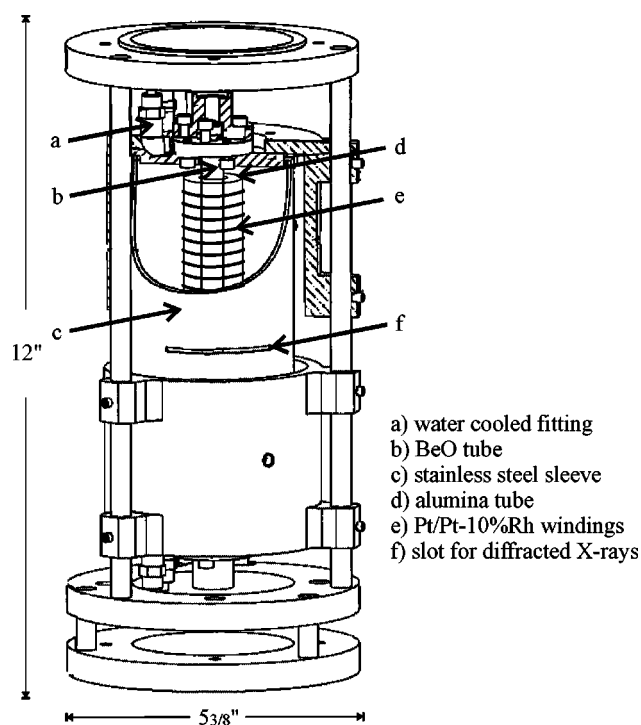


FIG. 1. Schematic of the high temperature furnace design.

(iii) Any sources of error that affect proper structure factor determinations must be addressed to allow for structural refinement. In practice, it is found that incomplete powder averaging is the primary source of error due to the extremely low angular divergence achievable with synchrotron beam-lines. As a result, sample rotation must be designed into the furnace in such a way as to not compromise thermal stability or atmosphere control. With these design goals in mind, an attempt has been made to address the experimental issues involved in developing a reliable system for performing high-resolution, Rietveld quality, high temperature powder diffraction.

II. FURNACE DESIGN

The furnace design consists of three basic units; the furnace, an outer frame for mounting and position adjustment, and a magnetically coupled rotating sample mount which attaches to one end of the tube furnace. A schematic of the basic furnace without the sample rotation attachment is shown in Fig. 1. The furnace is composed of Pt/Pt-10% Rh wire wound onto an Al_2O_3 tube. A BeO tube fits inside the Al_2O_3 tube and acts as the sample chamber. BeO was chosen for a number of reasons. First, it has a high melting point (2530 °C), low thermal expansion, and good chemical stability, allowing it to be used in a large range of sample environments (up to 1800 K in oxidizing, inert, or reducing atmospheres). Second, its low absorption at high x-ray energies provides for uniform thermal insulation surrounding the sample without excessive intensity loss. A control thermocouple placed inside the BeO tube is used to measure the temperature while the set point and ramp rate is remotely controlled with a Eurotherm 808 digital controller. An additional cylindrical layer of alumina-silica (Zircar SALI) insu-

lation surrounds the furnace core, and this in turn is contained in a stainless steel can to complete the basic furnace. A 3 mm diameter hole, to pass the incident beam, and a 3 mm wide slot, which passes scattered x rays at angles from 0° to $90^\circ 2\theta$, have been cut in the Al_2O_3 tube, SALI insulation, and stainless steel sleeve so that the BeO tube is the only attenuating material through which the x rays pass. The furnace has been designed as a scaled down version of standard tube furnaces which are routinely used in many research laboratories in order to mimic actual processing environments as closely as possible.

The furnace is set inside an aluminum frame with a spring loaded end ring which has been designed to snap easily onto the chi-circle of a standard Huber four circle goniometer, where it is then secured using the standard mounting holes. The furnace is adjustable within this frame in the x, y, and z directions to allow proper alignment with the diffractometer and beam axes. Symmetrically placed spring loaded pins assure that the sample tube position remains centered during thermal expansion of the furnace assembly. Water cooled fittings with O-ring seals are attached to either end of the furnace to provide attachments to thermocouple leads, vacuum and gas lines, and the rotating sample holder. Depending upon the particular sample, furnace atmosphere, and temperature range of interest, a variety of sample tubes can be used including quartz, MgO, Al_2O_3 , and BN. The low absorption of high energy x rays offers greater flexibility in choosing sample holders while still maintaining good sample to holder signal ratios.

Sample rotation is achieved by magnetically coupling the sample holder shaft to a rotating motor shaft. This isolates the drive motor from the sample space and avoids any possible compromise of the atmosphere integrity. A rotating motor shaft seal can easily produce small leaks which would be unacceptable for oxygen sensitive materials, while placing a motor within the sealed sample space could produce potential outgassing problems. A schematic of the assembly is shown in Fig. 2. Two sets of four $\frac{1}{4}$ in. diameter SmCo_5 magnets are used for the coupling. The sample can be either rotated continuously or rocked about some angular range. A maximum rotation speed of 1000 revolutions per minute is possible.

III. ATMOSPHERE CONTROL

A Sierra Instruments electronic flow controller was used for gas mixing and flow rate control. Using a divided gas flow, typical flow rates through the furnace ranged from 0.1 to 5 cm per minute. The oxygen partial pressure of the environment can be easily controlled for PO_2 sensitive samples such as high temperature oxide superconductors. For highly oxidizing materials, the furnace seals were checked with a helium leak detector. Helium leakage was below the sensitivity of the detector (10^{-6} mbar ℓ/s). In this case, the oxygen content of the sample space is limited by the purity of the incoming gas. For extremely oxidizing materials, quartz tubes containing sample powder and gettering material can

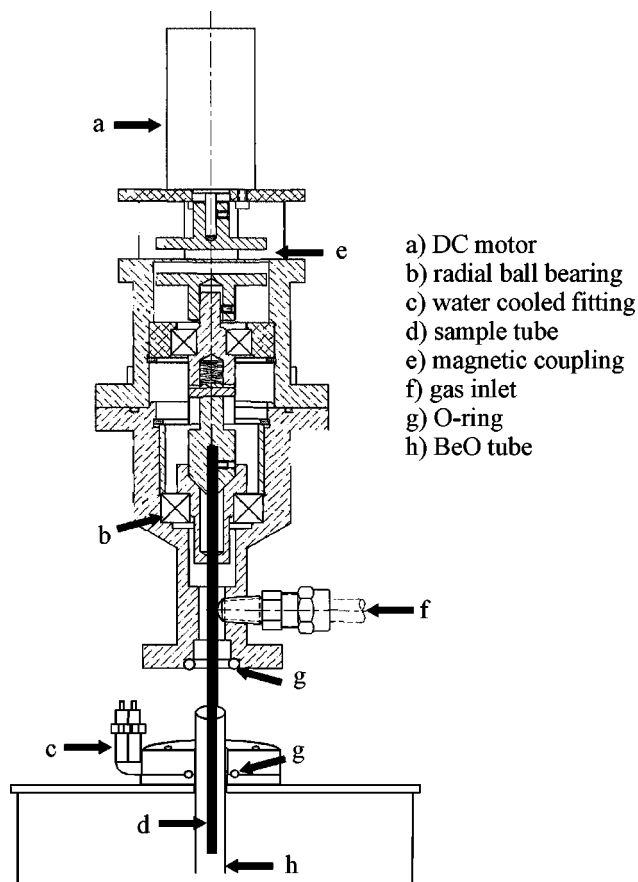


FIG. 2. Schematic of the magnetically coupled sample rotation attachment.

be vacuum sealed. Such samples holders were found to be very effective for preventing oxidation as well as for containing reactive liquids.

IV. TEMPERATURE CALIBRATION

The temperature calibration curve and gradient profile of the furnace were measured using a NIST traceable *R*-type thermocouple which has been calibrated to $\pm 0.1^\circ\text{C}$. This thermocouple was placed in the center of the sample position and its value recorded versus the control thermocouple value. This is shown in Fig. 3. Additional data points are given for the solid state transformation temperatures of BaCO_3 and SrCO_3 (NBS temperature standards, GM-760) as observed by *in situ* x-ray diffraction. Figure 4 shows the thermal gradient profile along the furnace tube axis at a series of temperatures. The probed length of the sample is typically between 1 and 2 mm which corresponds to a ΔT of less than 1°C across the illuminated sample length.

V. HIGH-RESOLUTION STEP SCANS

A. Diffraction geometry

Figure 5 shows a schematic of the optics used at the A2 line of CHESS for collecting data used in the structural refinements presented below. A Si(111) double-crystal monochromator was tuned to an energy of 60 keV using a calibrated solid state detector. The beam size was 2 mm in the horizontal and 1 mm in the vertical giving an incident flux on

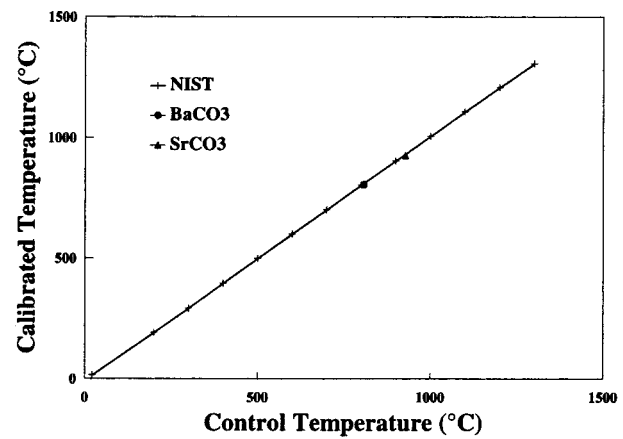


FIG. 3. Temperature calibration curve as measured by an NIST traceable standard thermocouple and *in situ* observation of solid state phase transformations of BaCO_3 and SrCO_3 .

the sample of approximately 10^{11} photons per second. A Si(111) analyzer crystal was used as an angular slit in front of a Na I detector. The analyzer and detector were scanned in the vertical scattering plane. The analyzer crystal was necessary to avoid resolution loss due to large sample diameters, and also minimizes sample displacement and fluorescence effects.¹ NBS standards were used to fit the wavelength and 2θ zero offset. Standards run at the beginning and end of the beam time showed the beam energy to be stable to within ± 7 eV. It was found that the 2θ zero offset was very sensitive to small misalignments of the analyzer crystal. Therefore, the analyzer crystal orientation was periodically checked by centering the crystal rocking curve on the direct beam. Scans used for Rietveld refinement were typically done with step sizes of $0.002^\circ 2\theta$ and counting times of 0.5–0.85 s per data point. The typical angular range recorded was 3° – $15^\circ 2\theta$, which corresponds to a range in reciprocal space of 1.6 – 8 \AA^{-1} for 60 keV x rays. This led to data collection times of approximately 1–2 h per scan. Scans taken with sample rocking were set up so that the two theta arm motion was coupled with the sample motor. The counting time for each step occurred over a 20° sample rotation at 4 rpm which alternated between clockwise and counterclockwise motion with each 2θ arm step.

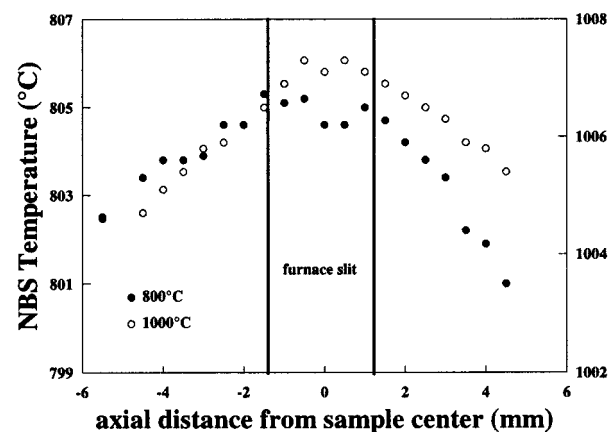


FIG. 4. Axial thermal gradient profile at sample position.

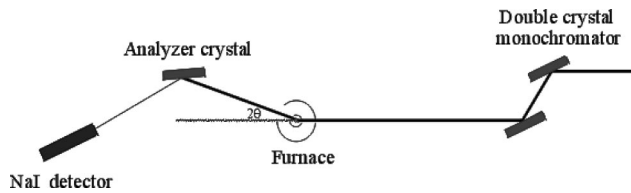


FIG. 5. Schematic of the beamline optics and diffraction geometry.

B. Peak profile shape and resolution

Previous work done at room temperature on high-resolution powder diffraction has demonstrated that diffraction peak shapes can be well described using a pseudovoigt function, which is a linear approximation to the convolution of Gaussian and Lorentzian functions.³ The functional form gives the intensity as a function of displacement from the peak center ($\Delta 2\theta$):

$$I(\Delta 2\theta) = I_0 \{ 2\eta/\Gamma [1 + 4(\Delta 2\theta/\Gamma)^2]^{-1} + 2(\ln 2/\pi)^{1/2} \times (1 - \eta)/\Gamma \exp[-4 \ln 2(\Delta 2\theta/\Gamma)^2] \} + I_B, \tag{1}$$

where I_0 is the integrated intensity, Γ is the full width at half maximum, η is the mixing parameter for determining the Gaussian/Lorentzian contribution, and I_B is the background intensity.

Individual peaks were fit to this function using the least squares peak fitting program PeakFit from Jandel.¹⁰ Figure 6 shows a fit to the (111) reflection from an NBS CeO₂ standard. The fit is quite good, and the peak shape is highly symmetric even at this low angle (3.74°). The CeO₂ standard should not exhibit significant sample broadening effects and therefore should give a fairly good indication of the instrumental resolution of the experiment. It has been shown¹¹ that in a nondispersive geometry the instrumental resolution function of a double-crystal monochromator and analyzer crystal is given by

$$\Gamma(\theta) = \{ \phi_v^2 (2 \tan \theta / \tan \theta_M - \tan \theta_A / \tan \theta_M - 1)^2 + \Gamma_{min}^2 \}^{1/2}, \tag{2}$$

where ϕ_v is the vertical divergence of the incident beam, θ_M and θ_A are the Bragg angles of the monochromator and ana-

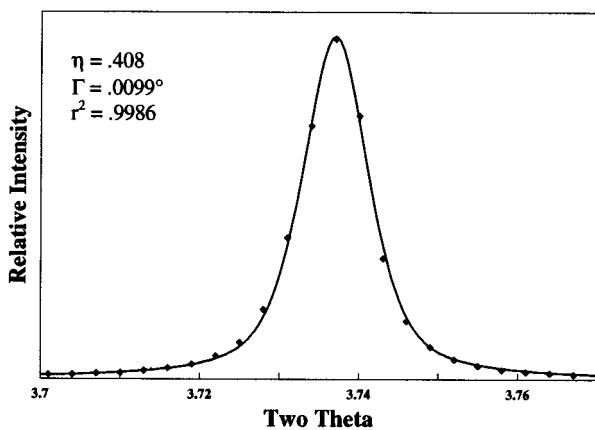


FIG. 6. (111) reflection from a CeO₂ standard fit to a pseudovoigt function.

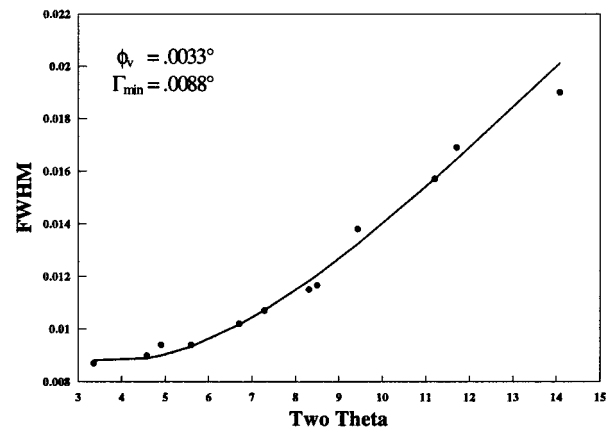


FIG. 7. CeO₂ reflection widths fit to the instrumental resolution function. ϕ_v is the vertical divergence of the white beam and Γ_{min} is the combined darwin width of the monochromator and analyzer crystals.

lyzer, respectively, and Γ_{min} is the natural darwin width of the crystals. Figure 7 shows the variation of reflection width with scattering angle for the CeO₂ standard. The solid line is a least squares fit of the data to Eq. (2).

C. Rietveld refinement

In Rietveld refinement, powder diffraction intensity data is fit using a least-squares algorithm to a function of the form:

$$Y_i = B_i + s \sum |F(hkl)|^2 \phi(\Delta 2\theta), \tag{3}$$

where B_i is the background intensity, s is a scale factor, the summation is over the complete set of contributing reflections at each data point, and $\phi(\Delta 2\theta)$ is the peak profile function.¹² A number of possible parameters can be fit which correspond to models of the sample structure and diffraction geometry. Among the parameters fit in this experiment were 2θ zero offset, x-ray wavelength, cell parameters, isotropic or anisotropic thermal parameters, variable atomic positions, background function, peak profile parameters, and a preferred orientation parameter. In addition, anomalous dispersion corrections were entered based on tabulated values. All

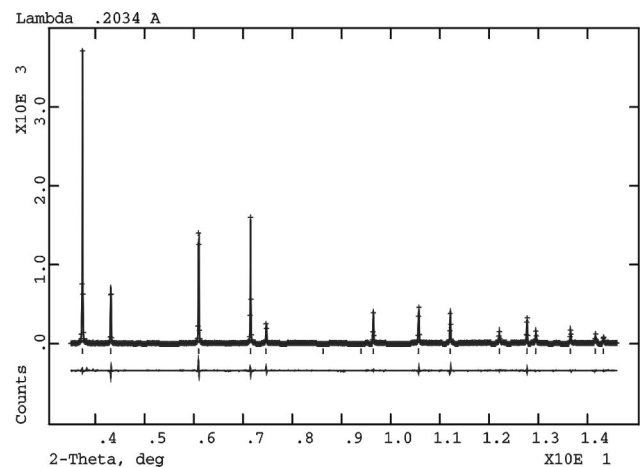


FIG. 8. Rietveld refinement plot of CeO₂ with residuals shown below. Regions containing peaks from the BeO furnace tube and MgO capillary tube were excluded from the refinement.

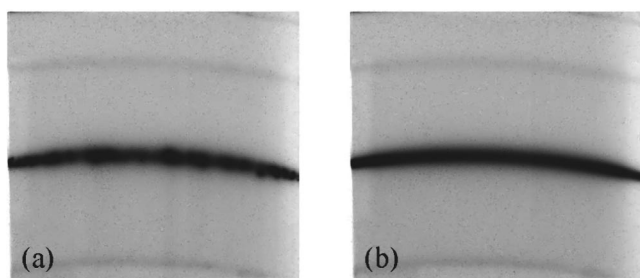


FIG. 9. CCD image of Fe_3Al powder (a) taken with stationary sample and (b) taken with sample rotation.

refinements were performed using GSAS.¹³ Diffraction peaks from the BeO furnace tube were excluded from the refinements. Due to the high resolution of this experiment, overlap with sample peaks was minimal, and the BeO peaks could be removed with minimal loss of sample reflection data.

CeO_2 (NBS standard 674a) was used as a wavelength and zero offset calibration standard by performing refinements with the cell parameter fixed at the NBS certified value. It was found that sample rotation was critical for successful Rietveld fitting. Refinement of the data set collected with a stationary sample was highly unstable and failed to converge. Data collected while rotating the sample about 20° per data point, though, successfully converged with a weighted residual of 10.56%. Figure 8 shows the refinement plot with residuals of this CeO_2 data set. The effect of sample rotation can be directly appreciated by comparing CCD images of diffraction rings from stationary and rotating samples (Fig. 9). The stationary sample gives a highly non-uniform intensity along the diffraction ring, which is typical of incomplete powder averaging. When the sample is rotated, though, the ring becomes uniform and the diffracted intensities can be used to reliably model structural parameters. It is clear that the lack of complete powder averaging in the case of the stationary sample introduced random errors into the structure factor measurements which prevented stable refinement.

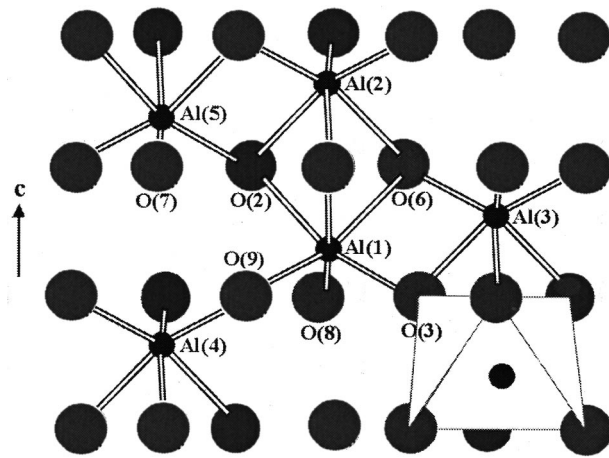
In order to test the ability to refine variable atomic positions, especially at high temperatures, Al_2O_3 powder (NBS standard 674a) was examined at room temperature, 873 K, and 1473 K. Data were collected for a 2θ range of 2.5° – 14.5° . Table I gives the refined parameters for these data sets. The most striking disagreement between the refined parameters and those reported previously in the literature is in

the thermal parameter values. Thermal parameters are notoriously difficult to measure accurately using x-ray powder diffraction data, since many of the systematic geometric and sample aberrations that can be introduced into powder diffraction data can be approximated by exponential functions which may be absorbed into the thermal parameter correction terms. For the case of a cylindrical sample which is completely bathed in the incident beam, the absorption correction can easily be taken into account.¹⁴ For this experiment, though, the vertical beam size was smaller than the sample diameter. In addition, slight precession during sample rocking further complicates the situation. For these reasons, we were unable to adequately correct for absorption effects. This may explain the lack of agreement between various experiments and the nonphysical negative values refined for some of the oxygen thermal parameters. The fact that the thermal parameters do increase with temperature suggests that at least qualitative trends in these values may be real. Smaller sample tube diameters are necessary to correct for this and to allow for quantitative thermal parameter determination.

The refined atomic positions show much better agreement with single crystal data,¹⁵ and there are clear trends when examining the high temperature structure. In the $R\bar{3}c$ structure of Al_2O_3 there are two variable atomic positions. Oxygen atoms are located at the position $(x, 0, \frac{1}{4})$ and are sixfold coordinated forming a distorted hexagonal close-packed structure. Al atoms are located at the position $(0, 0, z)$ and occupy $\frac{2}{3}$ of the octahedral interstitial sites. The refined $O(x)$ and $\text{Al}(z)$ parameters reveal subtle structural distortions with temperature. To our knowledge, there has been only one other measurement of the high temperature variable atomic positions in Al_2O_3 . That study was performed on a gas-flame heated single crystal at 2170 K¹⁶ and the results are consistent with the structural trends observed in our refinements. These structural changes can be understood in terms of distortions in the bond distances within and between Al–O sixfold coordinated polyhedra. Figure 10 shows a schematic of the coordinated polyhedral structure. Two AlO_6 octahedra share a common face which is perpendicular to the c axis. The Al(1)–Al(2) bond across this face is the nearest Al–Al distance in the structure. The Al atoms are displaced from the center of each AlO_6 octahedron away from the shared face and toward an empty interstitial site. This displacement becomes more pronounced with increasing temperature. This is clearly seen by examining changes in the

TABLE I. Refined parameters for Al_2O_3 data sets. Single-crystal data were taken with Mo $K\alpha$ radiation (Ref. 15). The data from Cox *et al.* (Ref. 3) were taken with synchrotron radiation on a 0.5 mm capillary.

	Single crystal (293 K)	Cox <i>et al.</i> (293 K)	This study (293 K)	This study (873 K)	This study (1473 K)
a (Å)	4.75999(3)	4.7586(1)	4.75957(4)	4.77953(4)	4.80754(4)
c (Å)	12.99481(7)	12.9897(1)	12.9926(3)	13.0551(3)	13.1383(3)
Al(z)	0.35219(1)	0.3518(1)	0.3528(1)	0.3531(1)	0.3533(1)
B(Al) (Å ²)	0.26(1)	0.68(5)	0.54	0.86	1.42
O(x)	0.30633(5)	0.3082(6)	0.3066(5)	0.3070(5)	0.3071(5)
B(O) (Å ²)	0.28(1)	0.71(7)	–0.26	0.16	0.42
Rwp		0.222	0.1300	0.1227	0.1209


 FIG. 10. Structure of Al_2O_3 viewed looking down the $[110]$ direction.

two independent Al–O bond lengths within each octahedron. In Fig. 11 the fractional change in the Al(1)–O(2)/Al(1)–O(9) bond mismatch is shown normalized to the room temperature values. The two Al–O distances are clearly diverging with increasing temperature. In addition, changes in the O atom site position tend to reduce distortions in the close-packed structure. The refined interatomic distances and bond angles are further summarized in Table II.

VI. TIME-RESOLVED IMAGE PLATE STUDY

Initial work on developing time-resolved high temperature diffraction was performed at the SRI-CAT 1-ID line at the Advanced Photon Source (APS). A Si(111) double-crystal monochromator was tuned to the Sm K absorption edge (46.834 keV). In order to achieve adequate time resolution, the analyzer crystal was abandoned in favor of an area detector. As a result, angular resolution is now limited by sample size. The practical consequence of this is a factor of 4 loss in angular resolution. In addition, we are now considerably more sensitive to misalignments in sample position as well as to incoherent background scattering. With this lower resolution, overlap between sample peaks and peaks from the BeO furnace tube becomes a concern. For this reason, an

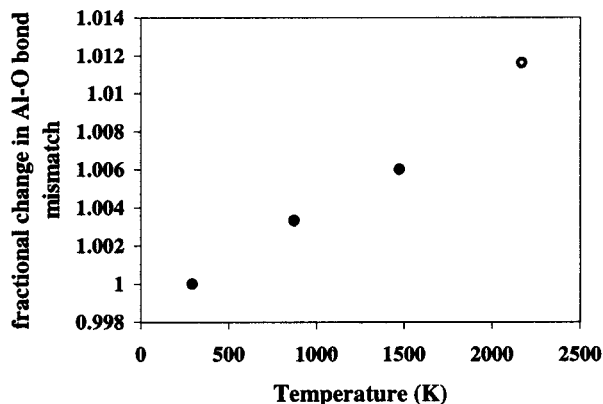


FIG. 11. Fractional change in Al(1)–O(2)/Al(1)–O(9) bond length mismatch normalized to room temperature. The value at 2170 K is taken from Ishizawa *et al.* (Ref. 16).

 TABLE II. Interatomic distances (\AA) and bond angles ($^\circ$).

	293 K	873 K	1473 K
Al(1)–Al(2)	2.672	2.692	2.715
Al(1)–Al(3)	2.794	2.807	2.825
Al(1)–Al(4)	3.210	3.220	3.236
Al(1)–Al(5)	3.499	3.514	3.535
Al(1)–O(2)	1.978	1.991	2.006
Al(1)–O(9)	1.850	1.856	1.865
O(2)–O(6)	2.528	2.542	2.557
O(2)–O(7)	2.864	2.875	2.891
O(2)–O(8)	2.621	2.633	2.650
O(2)–O(9)	2.725	2.737	2.753
Al(1)–O(2)–Al(2)	84.93	85.05	85.20
Al(1)–O(6)–Al(3)	93.68	93.67	93.67
Al(1)–O(9)–Al(4)	120.34	120.39	120.36
Al(1)–O(2)–Al(5)	132.04	131.96	131.91
O(2)–Al(1)–O(6)	79.41	79.32	79.21
O(2)–Al(1)–O(9)	86.32	86.33	86.33
O(9)–Al(1)–O(3)	101.44	101.53	101.62
O(2)–Al(1)–O(3)	163.87	163.75	163.61

amorphous silica tube was used instead of BeO. These are all necessary compromises in order to achieve real time measurements.

The detector configuration chosen for this initial experiment was a $20\text{ cm} \times 25\text{ cm}$ Fuji image plate which was scanned across a $1\frac{1}{2}\text{ mm}$ wide vertical slot. The time resolution of the experiment is effectively controlled by the width of the slit and the scanning speed. For this run, we kept the slit size constant at $1\frac{1}{2}\text{ mm}$ and varied the scanning rate between 0.02 and 0.2 mm/s, which corresponded to a time resolution of between 75 and 7.5 s. Measurements were typically taken at a constant heating rate so that a continuous temperature scale could be easily correlated with the image plate scan. For this experiment, the sample to plate distance was 70 cm which led to a collected angular range of 2° – 18° 2θ , and a resolution of 0.008° 2θ per pixel given a scanned

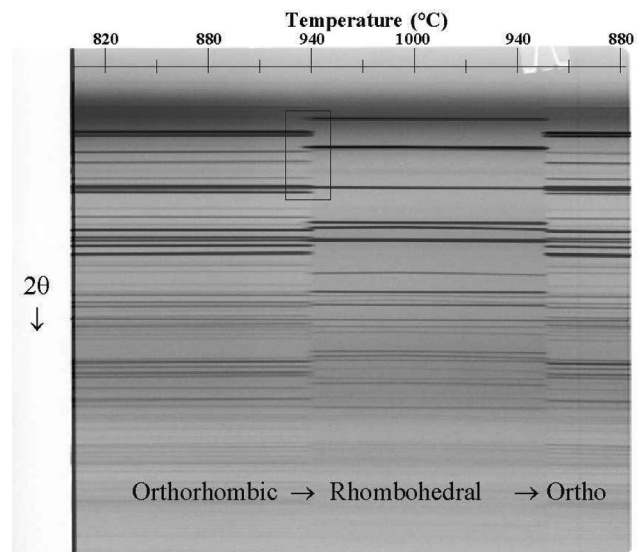


FIG. 12. Image plate scan of the reversible orthorhombic to rhombohedral phase transformation on heating and cooling of SrCO_3 . The ramp rate was $10^\circ\text{C}/\text{min}$ for both heating and cooling. The full height of the image plate corresponds to a 2θ range of 1.5° to 17.5° .

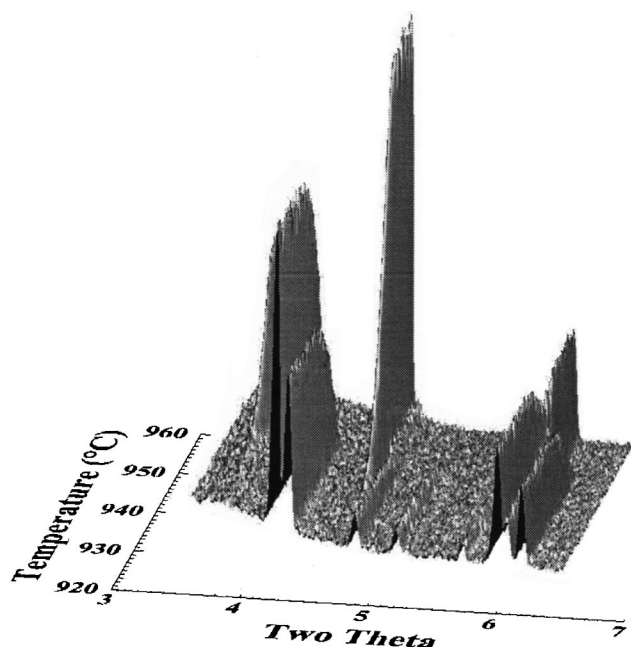


FIG. 13. Surface plot of the outlined phase transition region on heating from Fig. 12.

pixel size of $100\ \mu\text{m} \times 100\ \mu\text{m}$. Figure 12 shows a complete image plate scan taken during heating and cooling through the reversible solid state orthorhombic-rhombohedral phase transformation of SrCO_3 . The outlined area has been plotted as a three dimensional surface plot in Fig. 13. This plot clearly shows a narrow two-phase intermediate region. Such plots can be easily coupled with thermal analysis scans, allowing structural transformations to be correlated with thermal events as observed in differential thermal analysis (DTA), differential scanning calorimetry (DSC), or thermogravimetric analysis (TGA) measurements.

Data were collected on Al_2O_3 standard powder in order to test the potential for structural refinement with this technique. A cut of the image plate which corresponded to a time exposure of 7.5 s was processed to correct for aberrations due to the flat plate detector geometry. The processed data was then used for Rietveld refinement. Scattering from the amorphous silica furnace tube complicates the fitting, and a 26-term radial distribution function was necessary to properly model the background. The weighted residual of the final refinement was 6.87% (Fig. 14). This lower residual as compared to the high-resolution step scan refinements does not necessarily reflect a better structural fit, but rather is indicative of the higher background contribution to the image plate pattern. Despite the larger background and lower resolution, structural parameters could still be successfully fit. The $\text{Al}(z)$ and $\text{O}(x)$ variable atomic positions refined to values of 0.3521 and 0.3064, respectively. These values are in close agreement with the single-crystal data presented in Table I. The ability to collect high temperature Rietveld refineable diffraction patterns with a time resolution on the order of seconds opens up the possibility of observing subtle structural changes during phase transformations. In particular, transient metastable structures may be observable in the intermediate stages of kinetic processes.

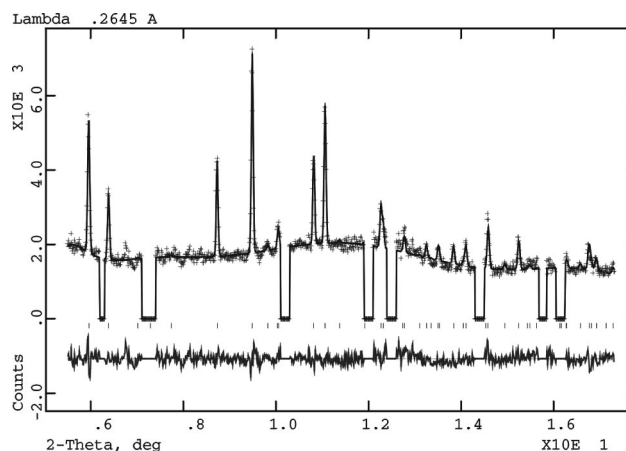


FIG. 14. Rietveld refinement plot of an Al_2O_3 powder pattern taken with a 7.5 s image plate exposure. Regions containing reflections from the MgO sample holder were excluded from the refinement.

VII. DISCUSSION

This furnace design has proven to be robust and reliable in the development of high temperature structural refinement techniques. The extremely low thermal gradients ($<1\ \text{°C}/\text{mm}$) across the probed sample length, as well as the ability to control the sample atmosphere demonstrate the robustness of this design. In addition, the use of Debye-Scherrer geometry is well suited to incorporating sample spinning, which we have found to be critical for powder averaging and reliable structural modeling. The use of high energy x rays in transmission assures full bulk sampling of the material; avoiding artifacts due to phase separation or surface effects. Coupled with area detectors, such as image plates or CCD cameras, this furnace design can be used for time-resolved measurements. Initial work with an image plate detector system has demonstrated that structural refinement with a time resolution on the order of seconds is achievable. Further work on developing techniques for time-resolved structural refinement of *in situ* kinetic processes is currently underway.

ACKNOWLEDGMENTS

The authors would like to acknowledge Kevin Dennis, Scott Bower, and Eric Deters for aiding in the furnace design and construction. The work at Ames Laboratory was supported by the U.S. Department of Energy through Iowa State University under Contract No. W-7405-ENG-82. The work at the Advanced Photon Source (APS) was supported by the U.S. Department of Energy, BES-Materials Sciences, under Contract No. W-31-109-ENG-38. The work conducted at the Cornell High Energy Synchrotron Source (CHESS) was supported by the National Science Foundation, under Award No. DMR-9713424.

¹J. B. Hastings, W. Thomlinson, and D. E. Cox, *J. Appl. Crystallogr.* **17**, 85 (1984).

²P. Thompson and I. G. Wood, *J. Appl. Crystallogr.* **16**, 458 (1983).

³P. Thompson, D. E. Cox, and J. B. Hastings, *J. Appl. Crystallogr.* **20**, 79 (1987).

⁴M. S. Lehmann, A. N. Christensen, H. Fjellvag, R. Feidenhans'l, and M. Nielsen, *J. Appl. Crystallogr.* **20**, 123 (1987).

- ⁵D. E. Cox, B. H. Toby, and M. M. Eddy, *Aust. J. Phys.* **41**, 117 (1988).
- ⁶F. Marumo, H. Morikawa, Y. Shimizugawa, M. Tokonami, M. Miyake, K. Ohsumi, and S. Sasaki, *Rev. Sci. Instrum.* **60**, 2421 (1989).
- ⁷S. E. Rasmussen, J. Jorgensen, and B. Lundtoft, *J. Appl. Crystallogr.* **29**, 42 (1996).
- ⁸F. Muller, I. Rannou, L. Duclaux, and J. M. Guet, *J. Appl. Crystallogr.* **30**, 557 (1997).
- ⁹J. Schreuer, A. Baumgarte, M. A. Estermann, W. Steurer, and H. Reifler, *J. Appl. Crystallogr.* **29**, 365 (1996).
- ¹⁰Peakfit v3.0, Jandel Scientific (1990).
- ¹¹P. Coppens and D. E. Cox, *Synchrotron Radiation Crystallography* (Academic, New York, 1992), Chap. 3, pp. 186–254.
- ¹²H. M. Rietveld, *J. Appl. Crystallogr.* **2**, 65 (1969).
- ¹³A. C. Larson and R. B. Von Dreele, Report LAUR 86-748, GSAS, Los Alamos National Laboratory, Los Alamos, NM, 1994.
- ¹⁴*International Tables for X-ray Crystallography*, Vol. III, edited by C. H. MacGilavry, G. D. Rieck, and K. Lonsdale (Knoch, Birmingham, 1959).
- ¹⁵L. D. Calvert, E. J. Gabe, and Y. Le Page, *Acta Crystallogr., Sect. A: Cryst. Phys., Diffr., Theor. Gen. Crystallogr.* **A37**, C314 (1981).
- ¹⁶N. Ishizawa, T. Miyata, I. Minato, F. Marumo, and S. Iwai, *Acta Crystallogr., Sect. B: Struct. Crystallogr. Cryst. Chem.* **B36**, 228 (1980).